Aerosol and Air Quality Research, 16: 2067–2084, 2016

ISSN: 1680-8584 print / 2071-1409 online
doi: 10.4209/aaqr.2015.07.0481

Particulate Matter Estimation from Photochemistry: A Modelling Approach Using Neural Networks and Synoptic Clustering

Michael Taylor[1*†], Adrianos Retalis[1], Helena A. Flocas[2]

[1] *Institute for Environmental Research and Sustainable Development, National Observatory of Athens, I. Metaxa and Vas. Pavlou, Penteli, Athens 15236, Greece*
[2] *Department of Environmental Physics and Meteorology, National and Kapodistrian University of Athens, Athens 15784, Greece*

ABSTRACT

We report on the development and validation of a neural network (NN) model of PM_{10} concentrations in terms of photochemical measurements of NO, NO_2 and O_3 and temporal parameters that include the day of the week and the day of the year with its sinusoidal variation. A long-term record (≈10 yr) from 2001–2012 (inclusive) assembled from measurements taken at 10 station nodes in the air quality monitoring network of the Greater Athens Area in Greece has been used. Eight synoptic categorizations of the circulation at 850 hPa were used to partition the data record, and to train individual NNs with Bayesian regularization using 90% of available data for different atmospheric conditions. The time series of PM_{10} estimates was then reconstructed from the partitioned output. As a control, a NN without synoptic clustering was trained on the same data. The remaining 10% of the data was used for testing the simulation performance. NN models with synoptic clustering achieved an average root mean square error (RMSE) ≈ 16 μg m^{-3} across the station nodes with an average index of agreement (IA) of 0.71 (somewhat better than the control network whose performance statistics were RMSE ≈ 17 μg m^{-3} and IA = 0.61, respectively). For routine measurements below the EU Air Quality Directive limit value of 50 μg m^{-3}, the average error is as low as RMSE ≈ 11 μg m^{-3} across the station nodes. NN models were found to strongly outperform analogous MLR models over all station nodes.

Keywords: Particulate matter; Photochemistry; Air quality; Synoptic classification; Neural networks.

INTRODUCTION

Epidemiological studies have established a clear association between human exposure to ambient air pollution and the risk of increased mortality (Dockery and Pope, 1994; Boezen *et al.*, 1999; Samet *et al.*, 2000; Davidson et al., 2005; Kassomenos *et al.*, 2008; Pope III *et al.*, 2009; Rückerl *et al.*, 2011; Raaschou-Nielsen *et al.*, 2013). In 2012 alone, ambient air pollution was responsible for 3.7 million deaths; 6.7% of total deaths that year (Brauer *et al.*, 2012). One of the most important components of air pollution is particulate matter (PM) having aerodynamic diameters up to 10 μm (PM_{10}) as this embraces both anthropogenic and natural pollutants (IPCC, 2013). While the highest concentrations of PM tend to be measured next to busy roads in megacities, the observation of relatively high values of PM_{10} values at urban background stations (Vardoulakis and Kassomenos, 2008), suggests that large proportions of the population are being exposed to this type of ambient air pollution (Dimitriou and Kassomenos, 2014). In addition to the important impact of PM on human health, high PM concentrations are known to be harmful to ecosystems (Grantz *et al.*, 2003) and strongly affect the balance between air quality and climate change (Unger *et al.*, 2010; Tai *et al.*, 2012; Barnes *et al.*, 2013; Hedegaard *et al.*, 2013; Mues *et al.*, 2013). The European Commission has issued legislation (Directive 2008/50/EC) involving limit values to help control the level of PM. Two limit values have been set for PM_{10}: i) the daily mean concentration of 50 μg m^{-3} should not to be exceeded more than 35 times per year and ii) the annual mean concentration should not exceed 40 μg m^{-3}, and a "health-based" target value has been set for $PM_{2.5}$ with an annual limit of 25 μg m^{-3}. It should be noted that there is currently no regulation for PM_1 despite calls by the scientific community (Gerasopoulos *et al.*, 2007). As we write, 195 countries are attending the 2015 UN Climate Change Conference (UNCCC) in the 11th session of the meeting of the parties to the 1997 Kyoto Protocol and 166 countries have submitted national commitments to reduce

† Now at Laboratory of Atmospheric Physics, Aristotle University of Thessaloniki, Greece

* Corresponding author.
E-mail address: mtaylor@auth.gr

their CO_2 emissions. Importantly, PM is absent from the agenda. This is despite assessments of the International Panel on Climate Change (IPCC, 2013) who have called for expansion of global air quality monitoring of the spatiotemporal distribution of PM.

PM levels show a great deal of spatial variability at the regional level (Hoek *et al.*, 1997; Kassomenos *et al.*, 2014) and also between and within large urban areas (Eeftens *et al.*, 2012; Van Poppel *et al.*, 2013; Kassomenos *et al.*, 2014). However, the sparsity of ground-based monitoring stations has cast doubt on the generality of results obtained from point sampling and has motivated a shift in the last decade towards satellite mapping of surface PM concentrations estimated from aerosol optical depth (AOD) retrieved by space sensors (Hoff and Christopher, 2009), from LIDAR vertical profile information (Boyouk *et al.*, 2010; Zeeshan and Oanh, 2014), or from simulations performed by global atmospheric chemistry models (Liu *et al.*, 2004; van Donkelaar *et al.*, 2006, 2010). The problem is that satellite estimates of surface air pollution need to be validated in pixels where coincident ground measurements exist. Indeed, the Surface PARTiculate mAtter Network (SPARTAN) described by Snider *et al.* (2015) has been initiated for precisely this purpose. In the context of satellite-derived PM models, it is important to note that the prediction of PM from AOD is accurate to only ≈ 30% (Hoff and Christopher, 2009) and that the precision of the measurement of AOD itself is estimated to be only ≈ 20% accurate. Furthermore, a substantial range of skill has been observed in linear regression models of estimated PM (obtained from AOD retrievals) on measured PM values, with correlation coefficients (R) varying greatly ($0.4 \leq R \leq 0.8$) both regionally and also with aerosol type (Engel-Cox *et al.*, 2004). As a result, such high levels of uncertainty have so far hampered the incorporation of such models in operational satellite retrieval of PM_{10} and/or $PM_{2.5}$ concentrations. Given that the spatial resolution of ground-based PM measurements is low and inhomogeneous, and that this limits the capacity for validating satellite-derived estimates, there is a need to supplement the SPARTAN network of ground-based measurements with independent estimates of PM. In this paper, we therefore develop and validate a data-driven approach for estimating PM_{10} directly from photochemical measurements and meteorological parameters since these are both more spatially representative and are also routinely recorded by station nodes in existing air quality monitoring networks .

In the context of meteorology, evidence is also growing with respect to the impact of atmospheric circulation and synoptic conditions on PM; in particular the role of long-range transport on elevated PM_{10} levels. In a study of PM in European capitals, Kukkonen *et al.* (2005) concluded that the vast majority of cases where PM_{10} values exceeded the EC Directive were related to the prevalence of specific meteorological conditions including high pressure systems and temperature inversions. A more important example is the appearance of extreme smog episodes in the Greater Athens Area (GAA) in Greece which has been found to be associated with stagnating and re-circulating air masses (Vardoulakis and Kassomenos, 2008). In a landmark study involving a statistical determination of the variables that Granger causes the variability in PM_{10} in the GAA, Sfetsos and Vlachogiannis (2010) established causal relationships between the prevailing weather conditions and the observation of elevated values of PM_{10}. This conclusion is also confirmed by the study of Yuval *et al.* (2012) who found that general levels of air pollutants and their spatial distribution are determined by the state of the atmosphere with most of the variability being associated with the atmospheric synoptic scale. These studies suggest that synoptic conditions should be a key element in the development of models of PM. For a survey of the role of meteorology on different PM size fractions (PM_{10}, $PM_{2.5}$ and $PM_{2.5–10}$) in the GAA used as the study region in this paper, we refer the reader to Pateraki *et al.* (2012). The GAA is an important location for air pollution studies since it is situated at an important global air pollution cross-road, and has a well established air quality monitoring network contributing a long-term (decadal) data record of measurements of meteorological parameters and atmospheric chemistry. While not meeting the population criteria of a megacity per se, pollutant concentrations in Athens have been found to rival cities having tens of millions of inhabitants (Kanakidou *et al*., 2011) and have emerged as a result of the impact of the 2008 financial crisis on household fuel bills and wood burning during the winter months (Vrekoussis *et al.*, 2013).

In constructing a model of PM in terms of chemical, meteorological and/or temporal parameters, it is important to understand how PM co-varies (i.e., correlates) with each of them. In relation to chemistry, a 2003 study in the GAA (Chaloulakou *et al.*, 2003a) found that annual Pearson product-moment correlations (R) between PM_{10} concentrations and routinely measured chemical variables were strong in the case of CO ($0.71 \leq R \leq 0.72$), NO and NO_x ($0.64 \leq R \leq 0.69$), moderate for SO_2 and NO_2 ($0.49 \leq R \leq 0.6$), weak to moderate for surface temperature ($0.39 \leq R \leq 0.46$), and moderately-negative (i.e., inversely correlated) for local wind speed ($–0.43 \leq R \leq –0.54$). The measurement of the variation of PM_{10} in 31 Chinese provincial capital cities using data from 286 monitoring sites (Xie *et al.*, 2015) found that the pairwise correlation between PM_{10} and O_3 was weak but that the correlation with CO was unstable (highly variable). These studies suggest that PM_{10} is dependent upon photochemical "markers" of ambient air pollution and fairly robust to standard meteorological parameters. In a very comprehensive study, Kukkonen *et al.* (2003) used 4 temporal variables (the hour, the day of the week and the sine and cosine of the day of the year) and a set of 34 meteorological variables (see Table 1 of Kukkonen *et al.*, 2003 for details) to construct a neural network (NN) 1-step ahead forecast model of PM_{10} in terms of time lagged values of PM_{10} and CO measured in downtown Helsinki. However, the performance skill of the NN was found to be too low to suggest its adoption for predicting spatial concentration distributions in the urban areas. A similar finding was obtained in the GAA where the impact of meteorological variables (ambient temperature, wind speed and direction, and relative humidity) and the day of the week as a temporal variable on the next-day prediction

Table 1. Description of the 20 station nodes of the air quality monitoring network in the Attica region contributing chemical measurement data during the ≈10 yr study period: 2001–2012 (inclusive) used in this work.

Abbrev.	Site Name	Source Type	Lat. (°N)	Long. (°E)	Elevation (m)
AGP	Agia Paraskevi	Suburban-Background	23.8194	37.9951	290
ATH	Athinas	Urban-Traffic	23.7268	37.9782	100
ALI	Aliartos	Background	23.1103	38.3752	110
ARI	Aristotelous	Urban-Traffic	23.7276	37.9880	95
GAL	Galatsi	Suburban-Background	23.7482	38.0203	154
GEO	Geoponiki	Suburban-Industrial	23.7068	37.9836	40
GOU	Goudi	Urban-Traffic	23.7674	37.9841	155
ELE	Elefsina	Suburban-Industrial	23.5384	38.0514	20
PAN	Zografou	Suburban-Background	23.7867	37.9696	245
THR	Thrakomakedones	Suburban-Background	23.7582	38.1435	550
KOR	Koropi	Suburban-Background	23.8790	37.9013	140
LIO	Liosia	Suburban-Background	23.6978	38.0768	165
LYK	Lykovrisi	Suburban	23.7888	38.0679	234
MAR	Marousi	Urban-Traffic	23.7874	38.0308	170
SMY	Nea Smyrni	Urban-Background	23.7130	37.9320	50
OIN	Oinofyta	Suburban-Industrial	23.6389	38.3062	100
PAT	Patission	Urban-Traffic	23.7330	37.9995	105
PIR	Pireas 1	Urban-Traffic	23.6452	37.9447	4
BIO	Pireas 2	Urban-Background	23.6527	37.9420	25
PER	Peristeri	Urban-Background	23.6884	38.0208	80

of PM_{10} with a NN led to only a marginal improvement in model skill as compared to a nonlinear autoregressive model that depended only on the lagged value of PM_{10} (Chaloulakou *et al.*, 2003b). There is an indication that synergistic approaches like the one adopted by Michaelides *et al.* (2011) whereby a NN was first deployed to classify synoptic patterns and this is then integrated with satellite AOD retrievals and time-lagged PM_{10} measurements in order to make one-step-ahead predictions of PM_{10}, have the potential to better capture the complex dynamics involved. So, while there are indications that NN models of PM_{10} have the potential to provide independent estimates of PM, a high skill recipe involving chemical inputs, temporal and meteorological variables has yet to be found. With this in mind, in this paper we exploit the long record of coincident observations of a broad range of air pollutants available at nodes in the GAA air quality monitoring network combined with the power of permutation analysis, synoptic clustering and NN models, to develop and test a general spatiotemporal model of PM_{10} that can potentially fill-in data gaps and support the development of more spatially representative prognostic models. To help maximize the likelihood of the uptake of the models we develop and their general utility, we will focus on photochemical measurements that are routinely made, and we use publicly-available maps of atmospheric circulation.

The rest of this paper is arranged as follows. The next section presents the data sources used in this work as well as a sensitivity analysis of the chemical constituents with multiple linear regression (MLR) used to determine the optimal combination of photochemical measurements in the NN models developed. This is followed by a description of the methodology adopted to construct and train NN solvers for PM_{10} from input variables that include photochemical measurements of NO, NO_2 and O_3, associated temporal parameters, and synoptic conditions together with training statistics. In this section, we also provide references on the Bayesian regularization procedure for nterested readers. In the results section, daily PM_{10} simulations are assessed using performance statistics for NNs trained with and without synoptic clustering and are compared against the results of the MLR model. The discussion section brings out our main findings and reports on the regimes of validity and general accuracy of the NN models. Finally, we conclude with a review of the potential of this approach for extending studies and data records of PM_{10}.

METHODS

In this work, data is drawn from 2 sources: *in situ* chemical measurements, and a daily synoptic categorization at the 850 hPa isobaric level. The dataset of coincident values was constructed from measurements taken at 20 station nodes in the GAA. In terms of geographical coverage, the GAA contains the capital of Greece, Athens, and spans a basin on the west coast of the Attica Peninsula in a small area of just 450 km^2 containing over 3.8 million inhabitants (35% of the total population of Greece). The GAA is subject to significant local sources of aerosol such as traffic, small to medium-scale industry, domestic combustion of fossil fuel and biomass, but, as we mentioned in the introduction, also long-range transport of atmospheric PM and ozone precursors. Surrounded by mountains on three sides, the topography of the area is unfavorable for the dispersion of air pollutants, and ventilation of the basin takes place only under northeasterly flow (Grivas *et al.*, 2008).

In Situ Chemical Data

A long (≈10 yr) data record (2001-2012 inclusive) of

concentration measurements of 10 different chemical species (CO, NO, NO_2, NO_x, O_3, SO_2, $PM_{2.5}$, PM_{10}, C_6H_6 and 'smoke') has been assembled from station nodes in the air quality monitoring network spanning the GAA. The characteristics of the sites is summarized in Table 1 and their geographical distribution is shown in Fig. 1 together with a "microarray" depicting data availability.

The spatial distribution of station nodes is not homogeneous and there is a much higher density of sites occupying the south-eastern part of the study region centred on the PAT site. Measurements of CO, NO, NO_2, NO_x, O_3, SO_2 and C_6H_6 are provided at the hourly timescale and measurements of $PM_{2.5}$, PM_{10} and smoke are provided daily. All measurements are in units of μg m^{-3} apart from CO which is in mg m^{-3}. There is also strong inhomogeneity in the array of chemical data as presented in the microarray of chemical measurements in Fig. 1. A first observation is that while chemical data for CO, NO, NO_2, O_3 and SO_2 are the most numerous (being in excess of 10,000 measurements at any given station node), the spatial representivity of CO is low with measurements only available at 8 of the 20 station nodes. The record of C_6H_6 measurements is volumous but only exists at the PAT station. Smoke measurements are only coincident with PM_{10} at the ARI site. The lack of spatial representivity and utility of C_6H_6 and smoke led us to exclude these chemical species from our study. A word of caution here is in order here. While there likely to be overlap between some of the chemical constituents present in smoke (e.g., NO_x) and the concentration of individual species measured, in this study, we do not attempt to decouple these effects due to the large uncertainty involved in not having spatially-representative data across the network of stations studied. Instead, we wish to emphasize the lowest common denominators - the routine measurements of

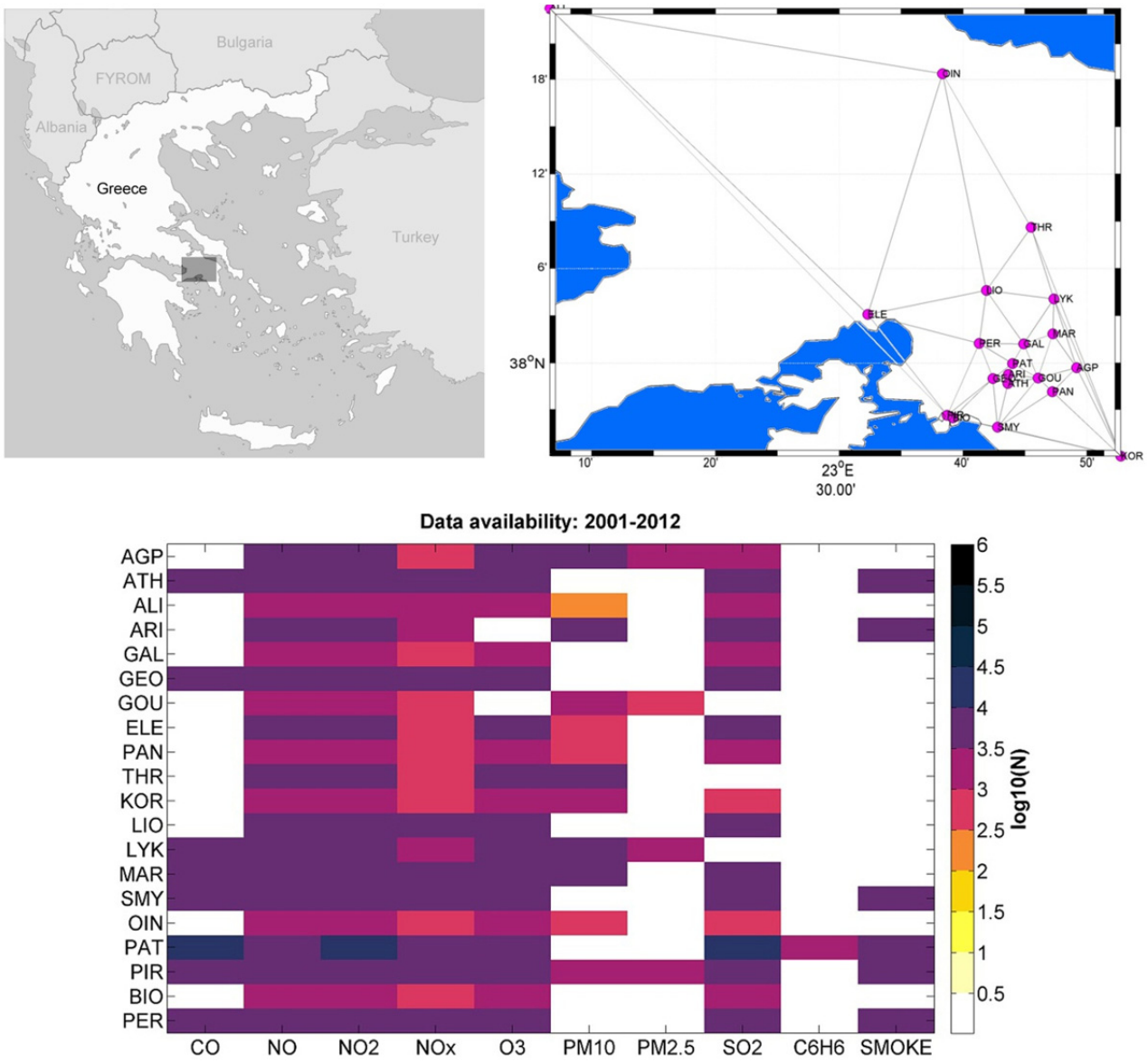

Fig. 1. *Upper Panels*: The Attica study region in Greece and the location of the 20 air quality monitoring station nodes. *Lower Panel*: The number (N) of chemical concentration measurements at each station for the period 2001–2012 (inclusive).

individual chemical constituents measured directly, in the hope of widening the applicability and generality of the model for estimation of PM in monitoring studies. The record of PM_{10} and $PM_{2.5}$ measurements is smaller than the photochemical data (numbering up to several 1000 records) since measurements are made daily, and are correspondingly less numerous than hourly data by a factor of 24. Only 4 station nodes (AGP, GOU, LYK and PIR) providing $PM_{2.5}$ data are coincident and overlap with the 12 station nodes providing PM_{10} data. Since our aim here is to construct and validate a multivariate model of the spatiotemporal variation of PM_{10} concentrations across the study region using a NN, synchronous data is required (i.e., it is necessary to supply simultaneous values of dependent and independent variables). This places a constraint on the number of data records and consequently the level of chemical detail. It is therefore necessary to quantify how the number of sites providing synchronous values varies with the number of different chemical species included. In order to do this, daily values and daily average values were selected. To be more specific, for the chemical species CO, NO, NO_2, O_3, $PM_{2.5}$, PM_{10} and SO_2, we extracted synchronous data for each of the 52 different chemical combinations that included PM_{10}. We then constructed a MLR model having the general form: $PM_{10} = f(CO, NO, NO_2, O_3, PM_{2.5}, SO_2)$ for each combination. To quantify the appropriateness of using each chemical combination for constructing a multivariate NN model of PM_{10} the value of the coefficient of determination (R^2) calculated from the goodness of fit of the MLR model as compared with the actual PM_{10} measurements, was used as a statistic. The rationale behind such an sensitivity analysis is to quantify and make objective the choice of chemical input data to be used for the construction of an NN model, i.e., the choice of explanatory variables.

Table 2 shows the results of this analysis for combinations of chemical species that provide synchronous data for at least 3 station nodes (so as to guarantee a minimum level of spatial representivity). Note that the number of input chemical species used in this pre-processing data compression step varies from 1 to 6 (the latter corresponds to the case of an input vector containing all of CO, NO, NO_2, O_3, $PM_{2.5}$ and SO_2, and which gave a goodness of fit value of $R^2 = 0.432$ at the PIR station).

Table 2 shows that there is a trade-off between potential model complexity (in terms of the number of different chemical species included) and the spatial extent of

Table 2. Sensitivity analysis on the chemical constituents. The value of the coefficient of determination (R^2) at each station node for input chemical species combinations corresponding to at least 3 station nodes (N). The value of the median value of R^2 calculated across contributing station nodes in each combination is provided and used to rank the input parameter combinations across all contributing stations.

Inputs	AGP	ALI	ARI	GOU	ELE	PAN	THR	KOR	LYK	MAR	OIN	PIR	N	Median
NO, NO_2, O_3, $PM_{2.5}$	0.61								0.66			0.40	3	0.61
NO, O_3, $PM_{2.5}$	0.61								0.64			0.36	3	0.61
NO, NO_2, $PM_{2.5}$	0.60								0.66			0.40	3	0.60
NO, $PM_{2.5}$	0.60								0.63			0.35	3	0.60
NO_2, O_3, $PM_{2.5}$	0.59								0.66			0.34	3	0.59
NO_2, $PM_{2.5}$	0.57								0.63			0.32	3	0.57
$PM_{2.5}$	0.57								0.56			0.29	3	0.56
CO, NO, NO_2, O_3									0.41	0.36		0.28	3	0.36
CO, NO, NO_2									0.40	0.35		0.28	3	0.35
CO, NO_2, O_3									0.38	0.33		0.26	3	0.33
CO, NO_2									0.38	0.33		0.27	3	0.33
O_3	0.16		0.45	0.34			0.23	0.03	0.47	0.60	0.02	0.33	9	0.33
CO, NO, O_3									0.29	0.35		0.28	3	0.29
NO, NO_2, O_3, SO_2	0.22	0.31			0.36			0.04		0.36	0.12	0.29	7	0.29
CO, NO									0.28	0.34		0.27	3	0.28
NO, NO_2, SO_2	0.09	0.29	0.44		0.26			0.04		0.35	0.11	0.27	8	0.26
NO, NO_2, O_3	0.22	0.30			0.25	0.24	0.16	0.07	0.41	0.35	0.05	0.26	10	0.25
CO									0.17	0.30		0.24	3	0.24
CO, O_3									0.17	0.30		0.24	3	0.24
NO_2, O_3	0.20	0.29			0.22	0.24	0.16	0.07	0.36	0.20	0.02	0.10	10	0.20
NO, NO_2	0.10	0.28	0.46	0.36	0.16	0.06	0.11	0.05	0.41	0.34	0.04	0.25	12	0.20
NO_2, O_3, SO_2	0.19	0.30			0.32			0.04		0.13	0.09	0.18	7	0.18
NO_2, SO_2	0.08	0.26	0.26		0.26			0.03		0.12	0.08	0.16	8	0.14
NO_2	0.09	0.26	0.22	0.35	0.16	0.02	0.11	0.05	0.36	0.19	0.01	0.09	12	0.13
NO, O_3, SO_2	0.13	0.10			0.16			0.04		0.36	0.11	0.29	7	0.13
NO, O_3	0.11	0.11			0.13	0.13	0.05	0.05	0.30	0.34	0.04	0.26	10	0.12
NO, SO_2	0.04	0.06	0.37		0.14			0.03		0.35	0.10	0.27	8	0.12
NO	0.02	0.07	0.41	0.23	0.08	0.00	0.03	0.04	0.30	0.34	0.04	0.24	12	0.08
SO_2	0.03	0.00	0.07		0.09			0.00		0.02	0.00	0.14	8	0.03

synchronous data available (in terms of the number of contributing station nodes). Within these constraints, the optimal multivariate model arising from this data pre-processing step is that corresponding to the highest value of N, and concurrently the highest value of median R^2, and involves the chemical species quadruplet: PM_{10}, NO, NO_2, O_3. This optimal data combination involves synchronous data from the 10 station nodes: AGP, ALI, ELE, PAN, THR, KOR, LYK, MAR, OIN and PIR. Note that, while the actual performance of the multiple linear model in terms of the magnitude of R^2 is not important in the context of the aim of this work - which is to develop a much more powerful and accurate model, it is a necessary pre-processing step for data compression in terms of allowed chemical complexity in the model being constructed. Since the need to maximize the spatial representivity of our model was a constraint in our study, rather than perform a correlation analysis at each site and report the magnitudes and signs of the impact of each explanatory variable on the modeled PM, we have opted instead to show the overall effect of the choice of explanatory variables on modeled PM_{10} at each station by ranking goodness of fit statistics (the coefficient of determination, R^2).

Synoptic Categories for Clustering

The classification of the synoptic scale atmospheric circulation we adopt derives from the manual scheme proposed by Kassomenos *et al.* (1998a). The scheme has already been employed with success in connection to air quality (Kassomenos *et al.*, 1998b), daily mortality (Kassomenos *et al.*, 2001) and urban heat islands over the GAA (Michalakakou *et al.*, 2002). More recently, Zagouras *et al.* (2012) automated the scheme by applying a new method based on graph theory. In particular, eight synoptic categories were identified based on the geopotential distribution at 850 hPa isobaric level and the flow direction. The 850 hPa isobaric level, representative of the low level troposphere, is preferable to the use of the surface geopotential, as it avoids topographical effects. The 8 categories are statistically-distinct and were found to be representive of the whole range of synoptic scale patterns over the Mediterranean region (Kassomenos *et al.*, 1998a), and are shown in Fig. 2.

In this study, the daily synoptic classification was applied to the GAA for the period 2001–2012 (inclusive) by employing the charts at 12:00 UTC derived from the European Meteorological Bulletin (EMB). The time series of daily synoptic conditions comprises a total of 4164 categorizations. The categories, the number of days where the atmospheric circulation corresponds to each category, and their descriptor are as follows:

- Synoptic category 1 (465 days): *South-Westerly Flow.* A trough is observed south-west of the GAA, resulting in south-westerly flow, being accompanied by advection of warm and moist air masses from Africa (Fig. 2(a)).
- Synoptic category 2 (401 days): *North-Westerly Flow.* When the trough has passed, a strong north-westerly flow is established over GAA. This category is characterized by strong cold air advection (Fig. 2(b)).
- Synoptic category 3 (396 days): *Long-Wave Trough.* Greece is dominated by a quasi stationary long-wave trough with its axis being positioned over GAA (Fig. 2(c)). This category is related to rainfall.
- Synoptic category 4 (465 days): *Closed Low.* This category is characterized by the presence of a closed low, being accompanied by intense winds, usually from the northern sector, and rainfall (Fig. 2(d)).
- Synoptic category 5 (235 days): *Zonal Flow.* The circulation is almost zonal over the GAA, resulting in a prevailing westerly flow (Fig. 2(e)) with considerably lower intensity in the warm period of the year.

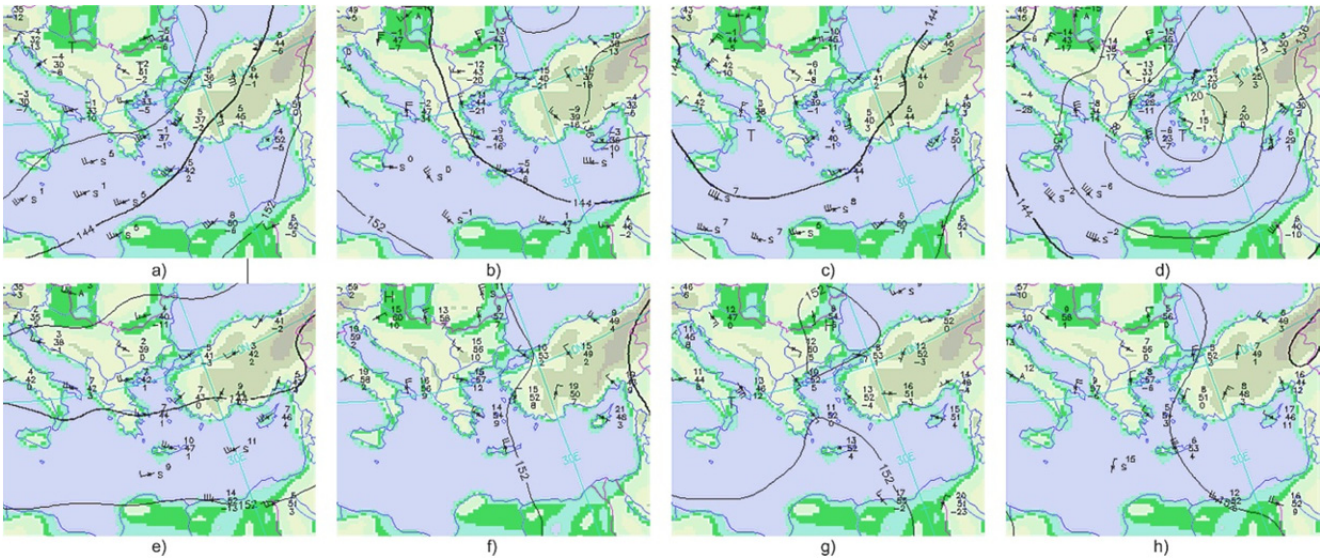

Fig. 2. Charts of the atmospheric circulation at the 850 hPa isobaric level (as derived from the European Meteorological Bulletin) for each of the 8 statistically-distinct synoptic categories over the Greater Athens Area (GAA): a) South-Westerly Flow, b) North-Westerly Flow, c) Long-Wave Trough, d) Closed Low, e) Zonal Flow, f) Open Anti-Cyclone, g) Closed Anti-Cyclone, h) High-Low, as per the taxonomy provided by Zagouras *et al.* (2012).

- Synoptic category 6 (1207 days): *Open Anti-Cyclone.* A large-scale ridge dominates over the Greek area, usually for several days (Fig. 2(f)). with weak variable winds, favouring the development of local flows.
- Synoptic category 7 (76 days): *Closed Anti-Cyclone.* This category is characterized by the presence of a closed anti-cyclone that extends over the major Greek area (Fig. 2(g)). This category appears with similar characteristics to the previous one, but causes weaker winds or calm conditions.
- Synoptic category 8 (919 days): *High–Low.* A ridge is combined with a trough over the central-eastern Mediterranean basin, resulting in rather complicated regimes over GAA. In the warm period, this category is mainly characterized by a strengthening of the pressure gradient and strong north-easterlies (the well known "Etesians") that blow over the Aegean Sea and into the GAA (Fig. 2(h)).

Cluster indices (1–8) corresponding to the synoptic category over the GAA on each day were then used to partition the coincident chemical data for PM_{10}, NO, NO_2 and O_3 from the 10 stations: AGP, ALI, ELE, KOR, LYK, MAR, OIN, PAN, PIR, THR into 8 subsets (one for each different synoptic category), under the assumption that the entire study region was governed by the same atmospheric circulation on any individual day.

Temporal Inputs

In their study to predict urban PM_{10} (and also NO_2) concentrations in central Helsinki using NN models, Kukkonen *et al.* (2003) found that it was necessary to incorporate the temporal/periodic variables into their NN models. The basis for including such periodic components in air quality forecasting is well established (Kolehmainen *et al.*, 2001) and we implicitly included the day of the week (DOW), the day of the year (DOY) and Sin(DOY) and Cos(DOY) into our model design. As mentioned in the introduction, the models we develop aim to address the lack of success in modeling PM_{10} in previous studies by: i) increasing the complexity of the range of chemical inputs used in the NN model and ii) by training different NNs for different and specific atmospheric circulation conditions. The subject of spatiotemporal prediction and forecasting of PM_{10} using lagged photochemical inputs will be the focus of a follow-up paper.

Statistics and Treatment of Errors

In Appendix A we present a brief description of the difference statistics used to assess the performance of the models developed in this work. While, measurement errors exist in the determination of the chemical concentration of each species and also in the assignment of synoptic categories to atmospheric circulation, it is assumed here that the observations are "error-free" so that the statistical framework described above is valid and can be applied. In this work then, the goodness of fit of NN model simulations to measurements of PM_{10} will be assessed with reference to the above statistics. We wish to note also that the above statistics will be calculated for measurements of PM_{10} above and also below the daily mean limit value of PM_{10} = 50 μg m^{-3} set by the EU Air Quality Directive.

Data pre-Processing

The sensitivity analysis applied to the chemical in situ data is an important step in model design to enhance the information content of the data. The dimensionality reduction it provides, like alternative approaches (e.g., principal components analysis or factor analysis) helps reduce parameter redundancy in the model. Another key step in preparing our data for use in model construction was normalization to remove potentially undesirable variances that arise from parameters having very different min-max ranges. In the neural network (NN) models we develop (described in the next section), all input and output matrices were preprocessed by mapping each parameter's mean to 0 and their standard deviations to 1 (i.e., to z-scores). In addition, a random number generator was used to ensure that identical initial weights were used in each run so that NN models with the same initial conditions could be compared. In particular, the twister algorithm (Matsumoto and Nishimura, 1998) based on Marsenne prime ($2^{19937}-1$) was called with a constant integer seed value to return a single uniformly distributed pseudo-random number in the interval (0, 1).

THE NEURAL NETWORK MODEL

In this section, we describe the construction, training and validation of a NN model for retrieval of PM_{10} estimates (outputs) from time series measurements of the daily photochemistry (NO, NO_2 and O_3) together with the periodic temporal variables: DOW, DOY, Sin(DOY) and Cos(DOY) as the input variables. For multivariate and temporally-static input-output data, a feed-forward NN having at least one layer of "hidden" neurons whose activation functions are general nonlinear sigmoidal functions (e.g., the *tanh* hyperbolic tangent function) has been proven to be able to operate as a universal function approximator (Cybenko, 1989; Hornik, Stinchombe and White, 1989). This means that, given enough hidden neurons and training data, such networks are capable of learning the exact mathematical relation between inputs and outputs. Fig. 3 presents the topology of a generic 3-layer multiple input, single output function approximating NN.

The exact mathematical equation relating the output to the inputs for this type of NN is given by the matrix equation (by analogy with the method described in Taylor *et al.* 2014):

$$Y = f^3\left(LW^{3,2} f^2\left(LW^{2,1} f^1\left(IW^{1,1} X + b^1\right) + b^2\right) + b^3\right) \quad (1)$$

The multiplication of the matrix $IW^{1,1}$ and the vector X is a dot product equivalent to the summation of all input connections to each neuron in the hidden layer. Eq. (1) is the continuous (nonlinear) functional approximation that relates the output vector to the matrix of input vectors.

For the NN models we construct in this work, Y = $[PM_{10}]^T$ and X = [NO, NO_2, O_3, DOW, DOY, Sin(DOY), Cos(DOY)]^T. The performance of NN models depends on their architecture (Bishop, 1995) and it is recommended that a

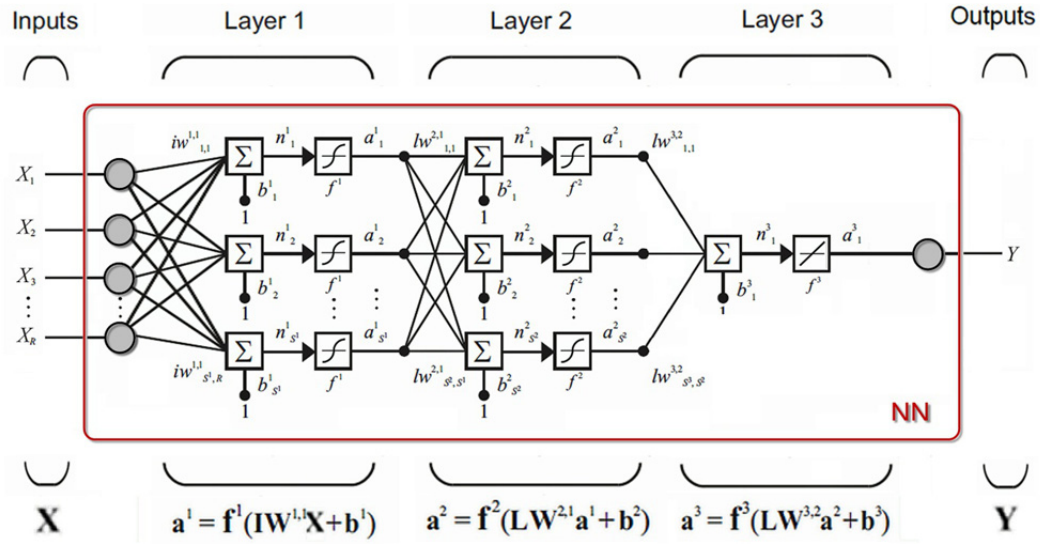

Fig. 3. Schematic showing the neural connectivity between input parameters and an output parameter in a multiple input, single output feed-forward NN having 2 layers of hidden neurons and a linear output layer.

sensitivity analysis is performed on the network parameters (Taylor *et al.*, 2014). To identify candidate optimal NN model structures, we initially trained a grid of NNs having a range of architectures: a) with 1 or 2 hidden layers of neurons, b) with between 10 and 40 neurons with *tanh* activation functions and c) with the proportion of training data varying between 70% and 90%. The NN models were coded using MATLAB's object-oriented scripting language in conjunction with its Neural Network Toolbox (Beale *et al.*, 2015). The size of the available data record is 17,760 coincident input-output vectors. 90% of the dataset (16,021 records) was used for NN training and the remaining 10% of the dataset (1,776 records) was used for simulation (see the Results section). The same training data was used in training each NN in the grid of different architectures and the number of learning iterations was set to 100.

The training algorithm used for the NN models developed in this study is Bayesian regularization using a Laplace prior (Williams, 1995) based on the Bayesian framework described by Mackay (1992). Bayesian regularization converts a nonlinear regression into a "well-posed" statistical problem by minimizing a linear combination of squared errors and weights and modifies the linear combination so that at the end of training the resulting network has good generalization qualities (Beale *et al.*, 2015). Bayesian regularization in MATLAB automates the determination of the optimal regularization parameters in its NN training function "*trainbr*" and takes place within the Levenberg-Marquardt algorithm where back-propagation is used to calculate the Jacobian of performance with respect to the weight and bias variables (Beale *et al.*, 2015). In line with the guidance of MATLAB's Neural Network Toolbox User's Guide (Beale *et al.*, 2015), we scaled all network inputs and targets to the range [–1,1] during training and then inverted outputs back to their true scales for application of the difference statistics described in Appendix A. For mathematical detail of the statistical regularization procedure implemented by MATLAB's "*trainbr*" NN training function we refer the reader to Williams (1995) and Mackay (1992). Bayesian regularization is well suited to complex/nonlinear problems involving a sizeable number of hidden neurons (e.g., > 10) and deep learning (2+ layers of hidden neurons) where, by restricting the magnitudes of weights, this method avoids overfitting. By optimizing the model parameters, it also has better generalization properties that other NN learning algorithms that may overfit or get trapped in local minima. Indeed, this was the main driving force behind our choice of Bayesian regularization - i.e., it was found to perform much better than three other standard back-propagation training algorithms (the Levenberg-Marquardt algorithm "*trainlm*", the resilient back-propagation algorithm "*trainrp*" and the Scaled Conjugate Gradient algorithm "*trainscg*" training functions in MATLAB). In contrast to the high target versus output correction values obtained with Bayesian regularizarion training (R = 0.97 for the optimal NN in Table 3), the other algorithms achieved much lower values in the range $0.52 \leq R \leq 0.73$ for the optimal NN architecture (2 layers of 30 hidden neurons). We will see in the results section that NN models trained with Bayesian regularization strongly outperform analogous MLR models (see Table 11) and we recommend that this scheme is adopted for problems of similar complexity.

For each NN, the back-propagation optimization algorithm (Rumelhart *et al.*, 1986) then proceeded to minimize the mean squared error (MSE) calculated from the difference between NN-derived PM_{10} outputs (y_i) and target PM_{10} measurements (t_i) in the validation dataset (100% - training %):

$$MSE = \frac{1}{N}\Sigma_{i=1}^{N}\left(t_i - y_i\right)^2 \quad (2)$$

Table 3 shows the results of the sensitivity analysis we performed on the parameters of the generic NN.

Table 3. Validation performance of a grid of NN architectures with: a) 1 or 2 hidden layers of neurons with hyperbolic tangent (*tanh*) activation functions, b) between 10 and 40 neurons in each hidden layer, and c) the proportion of training data varying between 70% and 90%. The optimal NN architecture is indicated by **.

Hidden Layers	Hidden Neurons	Training %	MSE	R
1	10	70	282.4	0.493
1	10	80	275.3	0.509
1	10	90	272.6	0.516
1	20	70	268.9	0.524
1	20	80	267.2	0.528
1	20	90	263.5	0.536
1	30	70	250.2	0.567
1	30	80	249.1	0.569
1	30	90	246.9	0.574
1	40	70	261.8	0.541
1	40	80	260.0	0.544
1	40	90	258.8	0.547
2	10	70	107.7	0.892
2	10	80	101.6	0.906
2	10	90	98.5	0.913
2	20	70	94.8	0.922
2	20	80	92.4	0.927
2	20	90	90.6	0.931
2	30	70	76.0	0.964
2	30	80	74.8	0.967
**2	**30	**90	**74.0	**0.969
2	40	70	90.4	0.932
2	40	80	88.9	0.935
2	40	90	87.1	0.939

For this grid of NNs and input-output data, the optimal architecture corresponds to a NN containing 2 hidden layers of 30 neurons when 90% of the data is used for training and 10% is used for validation. This reflects the fact that the relation between PM_{10} and the photochemistry is highly complex and nonlinear. The relative success of 3-layer NNs (i.e., containing 2 layers of hidden neurons) over 2-layer NNs supports the notion that deeper learning is required for this particular problem. This is also confirmed to some extent by the relatively large number of 30 neurons needed despite there being only a single output parameter and 7 input parameters. Having established an appropriate NN architecture, we then proceeded to train NNs for each synoptic cluster as described in the next section.

NN Training

Since daily atmospheric circulation over the study region was classified into 8 categories, it was necessary to train a total of 8 NNs. For each NN, the training dataset comprises complete records of daily-averaged values of NO, NO_2 and O_3 together with the associated day of the week (DOW; an integer index running from 1 to 7 starting on Sunday), the day of the year (DOY; an index running from 1 to 365 or 366 in the case of a leap year) and the sine and cosine of the DOY as inputs, together with the daily values of PM_{10} as the output assembled from coincident measurements at the 10 station nodes: AGP, ALI, ELE, PAN, THR, KOR, LYK, MAR, OIN and PIR in the air quality monitoring network during the period 2001–2012 (inclusive). As such, each of the NN models has 7 input variables and 1 output variable. The indices of each synoptic category were then used to partition the data into 8 subsets. Each subset was further partitioned into data used for NN training and ("unseen") data used for NN validation (the results of which are presented in the next section). For each synoptic category, a search was performed in each of the 12 years of the study period (2001–2012 inclusive) and 90% of the indices were stored for training while the remaining 10% of the indices were stored for validation. In total, 8 sets of training and validation indices were produced. For each category, the indices were then used to extract coincident chemical measurements together with their associated temporal variables. Fig. 4 shows the progression of training for the 'zonal flow' (Cluster 5) NN towards convergence at the horizontal asymptote for the "best" validation MSE after 100 epochs of back-propagation learning using Bayesian regularization. At this point where the slope of the validation MSE approaches zero, the effective number of parameters used in the regularization has converged. Fig. 4 shows that a high level of correlation has been achieved between target measured values of PM_{10} and the NN outputs with a Pearson product-moment correlation coefficient, $R = 0.944$. Robust regression was performed using the method of Theil (1950) and Sen (1968). The training results and associated statistics for each of the 8 synoptically-clustered NNs (labelled "NN1" to "NN8") are presented in Table 4. The variation of linear and nonlinear average error and goodness of fit statistics are also presented in Fig. 4.

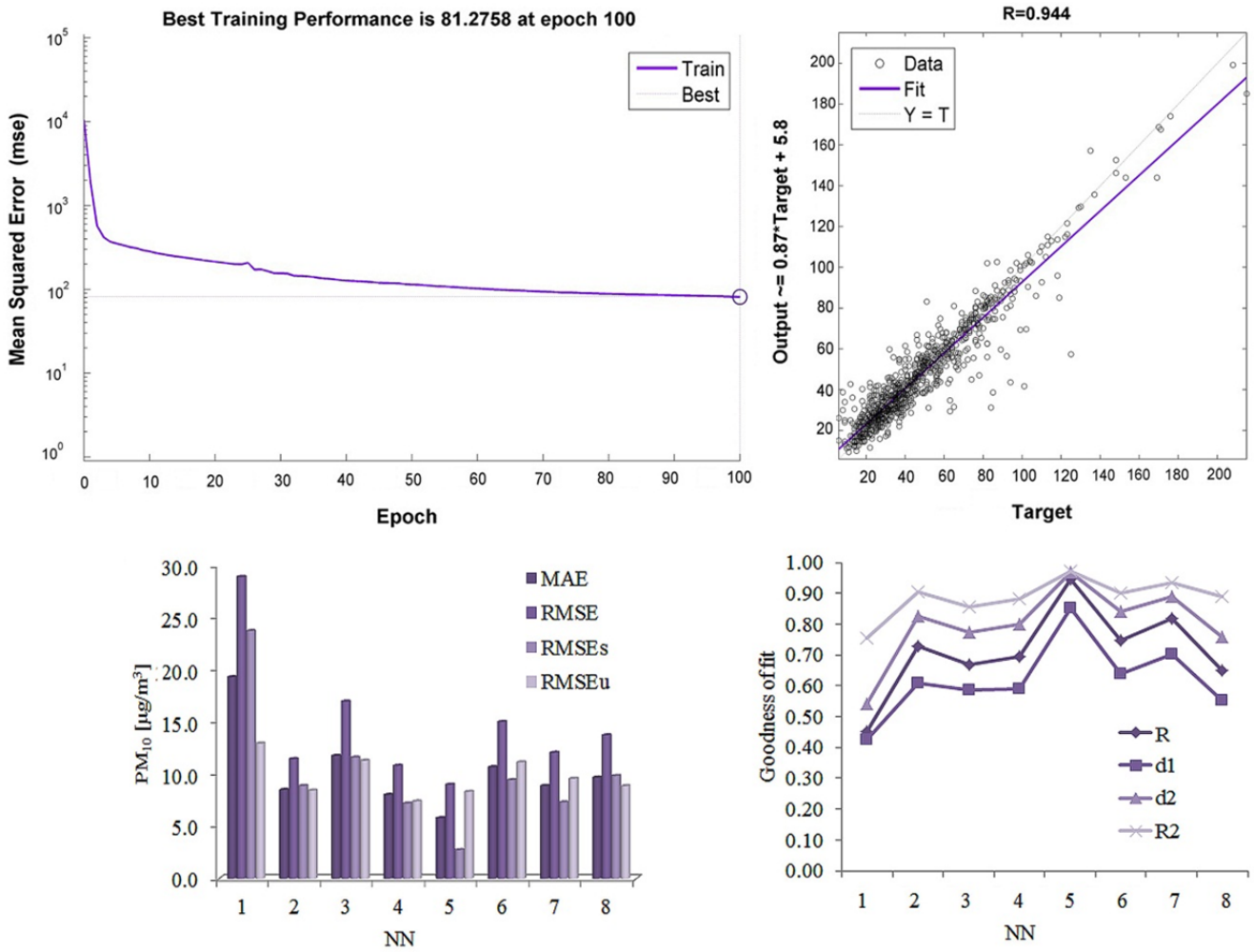

Fig. 4. *Upper Left:* Training of the 'zonal flow' (Cluster 5) NN showing how the MSE varies with back-propagation iteration (epoch). This NN has 2 layers of 30 hidden neurons with *tanh* activation functions and is trained with Bayesian regularization with a goal for the back-propagation cost function set to 1/100th of the total variance of the targets. *Upper Right:* A high level of correlation has been achieved between target measured values of PM_{10} and the NN simulation outputs (Pearson product-moment correlation coefficient, R = 0.944). *Lower Left*: Linear and nonlinear average error statistics for the 8 NNs corresponding to the partitioning of the data by synoptic category. *Lower Right:* Linear and nonlinear goodness of fit statistics for each trained NN.

Table 4. Statistics associated with training each of the 8 synoptically-clustered NNs (NN1 to NN8). In the table, N is the number of daily values assembled from coincident data drawn from the 10 station nodes and $N(> 50)$ is the number of values which exceed the limit set by the EU Air Quality Directive (2008/EC/50). The proportion of the data which are in excess of this limit is also given as a percentage. R is the Pearson Product-Moment Correlation coefficient from the regression of NN outputs on measured values. All other statistical quantities are described in the last section.

	N	R	μ_O	s_O	μ_P	s_P	b	MAE	RMSE	$RMSE_s$	$RMSE_u$	d_1	d_2	R^2
NN1	1688	0.45	48.3	32.4	48.4	14.3	0.0	19.3	28.9	23.8	13.0	0.42	0.54	0.75
NN2	1512	0.73	32.9	16.7	32.5	12.1	–0.4	8.5	11.5	8.9	8.5	0.61	0.83	0.90
NN3	1431	0.67	38.3	22.9	38.3	15.0	0.0	11.8	17.0	11.6	11.3	0.59	0.77	0.86
NN4	1791	0.70	27.9	15.1	27.9	10.3	0.0	8.0	10.8	7.2	7.4	0.59	0.80	0.88
NN5	907	0.94	46.6	27.4	46.4	25.2	–0.2	5.8	9.0	2.7	8.3	0.85	0.97	0.97
NN6	4851	0.75	42.4	22.7	42.3	16.8	0.0	10.7	15.0	9.5	11.2	0.64	0.84	0.90
NN7	333	0.82	42.7	21.1	42.5	16.7	–0.2	8.9	12.1	7.3	9.6	0.70	0.89	0.94
NN8	3508	0.65	37.1	18.1	37.1	11.6	0.0	9.7	13.7	9.9	8.9	0.55	0.76	0.89
Mean	2003	0.71	39.5	22.0	39.4	15.3	–0.1	10.3	14.8	10.1	9.8	0.62	0.80	0.89
St. Dev. (SD)	1468	0.14	6.9	5.7	6.9	4.7	0.2	4.0	6.2	6.1	1.9	0.12	0.12	0.06
Mean + 2SD	4938	1.00	53.3	33.5	53.2	24.6	0.2	18.4	27.3	22.3	13.5	0.87	1.00	1.00

NN5, corresponding to the case of 'zonal flow' (Cluster 5), presents the lowest linear and nonlinear measure of average error (MAE, RMSE, $RMSE_s$ and $RMSE_u$) and concurrently the highest values of the linear and nonlinear goodness of fit statistics (R, d_1, d_2, R^2). In order to assess whether or not partitioning of the data into synoptic categories and training a NN for each category offers an advantage over not using synoptic clustering (i.e., that taking meteorology into account provides a computational benefit), we also trained an additional NN without clustering using exactly the same input-output vectors (i.e., using 90% of the data from each synoptic category and then accumulation of the input-output vectors over all clusters). In order to be able to directly compare this "unclustered" NN which we label "NNU" with the 8 synoptically-clustered NNs, we recombined the simulated outputs from NN1 to NN8 into a single matrix of input-output vectors which we label "NNC". The statistics associated with NNC reflect the mean training performance over all 8 synoptically-clustered NNs. Table 5 shows the statistics associated with these two models.

The statistics for the NNs presented in Table 5 are based on the largest available sample of coincident data (N = 16021 daily input-output vectors). The training performance is reasonably good in both cases (e.g., the linear and nonlinear average error measures MAE, RMSE, $RMSE_s$ and $RMSE_u$ are in the range 10.06 to 18.04 μg m^{-3}, and the linear and nonlinear goodness of fit statistics R, d_1, d_2 and R^2 are in the range 0.56 to 0.88). Some slight improvement is apparent in the case of NNC suggesting that the use of synoptic clustering appears to offer some benefit. The simulation performance of the NNs is tested by feeding the trained NNs with unseen data (i.e. the 10% of the datasets not used during network learning). In the next section we evaluate the performance of the NN model by comparing simulated PM_{10} outputs against daily measurements from station nodes in the air quality monitoring network.

RESULTS

As a result of applying the methodology described in the previous section, a total of 9 NNs were trained (one for each of the 8 synoptic categories plus one without clustering). In each case, 90% of the dataset was used for training. In order to assess the simulation performance of the NNs, the remaining 10% of the dataset containing daily photochemical measurements: NO, NO_2, O_3 and associated temporal variables (DOW, DOY and the sine and cosine of DOY) coincident with PM_{10} measurements and synoptic categories at the station nodes: AGP, ALI, ELE, PAN, THR, KOR, LYK, MAR, OIN and PIR, was used. As for the NN training, cluster indices for synoptic categories were used to divide the data into 8 subsets (one for each synoptic category). The input vectors in each of the subsets were then fed to each of the 8 synoptically-categorized NNs to simulate daily PM_{10} values. The time series at each station node was then reconstructed from the simulated outputs for each synoptic category with reference to the associated cluster indices. Since coincident input-output vectors are used at every stage, simulation performance was assessed using the statistical difference measures described earlier. For the case of the NN trained without synoptic clustering (NNU), PM_{10} simulations and coincident measurements at each station node are directly compared without the need to perform time series reconstruction using cluster indices. In addition to the calculation of average error and goodness of fit statistics for time series at each station node, we have also flagged PM_{10} measurements that are in excess of the EU Air Quality Directive limit value of 50 μg m^{-3} so as to assess the performance of the NNs on routine values that are not outliers (in the sense that they exceed a limit value). In Table 6 we present statistics for simulated PM_{10} values obtained with the NN trained without synoptic clustering (NNU) for the data points at each station node. In Table 7 we present analogous statistics for data points that are below the limit value.

In Table 8 we present performance statistics associated with the reconstructed time series of PM_{10} simulations obtained from the output of the 8 synoptically-clustered trained NNs at each station node (NNC). Table 9 presents analogous statistics for data points that are below the limit value.

In order to assess whether or not partitioning of the data into synoptic categories and training a NN for each category offers an advantage, we present the simulation results from the NN trained without clustering for data accumulated across all station nodes ("NNU") with that resulting from simulation with the 8 synoptically-categorized NNs: NN1 to NN8 ("NNC"). Table 10 shows the statistics associated with these two simulations.

While comparable in performance, both NN models strongly improve on the results of the MLR model of PM_{10} where the median R^2 value across the 10 station nodes was found to be only 0.25 (see the entry for NO, NO_2, O_3 in Table 2). Table 11 shows that this improvement is systematic across all station nodes.

DISCUSSION

Comparison of NN estimates against measured values of PM_{10} across 10 station nodes in the air quality monitoring network of the GAA using photochemical inputs and associated temporal variables over the 2001–2012 (inclusive) study period, suggests that PM_{10} can be retrieved at the daily timescale with some confidence. This is true both for

Table 5. Statistics associated with training a NN without synoptic clustering ("NNU") and by reconstructing the data from aggregation of the simulations from the 8 synoptically-clustered NNs ("NNC").

	N	R	μ_O	s_O	μ_P	s_P	b	MAE	RMSE	$RMSE_s$	$RMSE_u$	d_1	d_2	R^2
NNU	16021	0.62	39.40	22.93	39.22	14.18	–0.19	12.02	18.04	12.47	11.32	0.56	0.73	0.84
NNC	16021	0.71	39.40	22.93	39.16	16.08	–0.05	10.66	16.02	10.06	11.39	0.62	0.81	0.88

Table 6. Statistics associated with PM_{10} simulations obtained from NNU at each station node compared with measured values.

	N	R	μ_O	s_O	μ_P	s_P	b	MAE	RMSE	$RMSE_s$	$RMSE_u$	d_1	d_2	R^2
AGP	304	0.53	32.45	19.18	33.54	9.13	1.09	11.40	16.33	13.39	7.81	0.44	0.62	0.81
ALI	26	0.69	29.42	9.96	31.56	7.45	2.13	5.84	7.37	5.50	5.27	0.58	0.79	0.94
ELE	27	0.54	42.41	15.72	43.03	8.67	0.63	11.22	12.98	11.48	7.22	0.43	0.66	0.92
PAN	49	0.77	25.49	11.46	30.75	6.94	5.26	7.41	9.11	7.67	4.40	0.53	0.77	0.89
THR	329	0.39	30.06	19.93	29.42	7.29	–0.64	10.27	18.31	14.83	7.08	0.42	0.44	0.74
KOR	134	0.15	30.22	26.03	30.09	5.25	–0.13	12.10	25.68	21.92	6.10	0.28	0.17	0.58
LYK	346	0.64	49.23	24.17	43.45	13.28	–5.78	13.05	19.54	15.80	10.31	0.56	0.71	0.87
MAR	304	0.57	46.99	26.28	44.48	17.20	–2.51	13.66	21.77	14.81	14.25	0.58	0.71	0.84
OIN	60	0.40	41.48	23.28	36.99	9.19	–4.49	14.30	21.66	21.05	8.46	0.40	0.49	0.79
PIR	197	0.55	45.86	18.50	54.32	13.92	8.46	14.56	18.02	14.37	11.81	0.43	0.69	0.87
Mean	178	0.52	37.36	19.45	37.76	9.83	0.40	11.38	17.08	14.08	8.27	0.47	0.61	0.83
SD	134	0.18	8.70	5.73	8.26	3.75	4.27	2.89	5.78	5.12	3.05	0.10	0.19	0.10
Mean + 2SD	446	0.88	54.76	30.92	54.28	17.33	8.94	17.15	28.63	24.33	14.38	0.66	0.98	1.00

Table 7. Statistics associated with PM_{10} simulations obtained from NNU compared with measurements which are below the EU Air Quality Directive limit value of 50 μgm^{-3}.

	N ($PM_{10} < 50$)	R	μ_O	s_O	μ_P	s_P	b	MAE	RMSE	$RMSE_s$	$RMSE_u$	d_1	d_2	R^2
AGP	258	0.47	25.98	9.40	31.94	7.21	5.95	8.67	10.57	8.32	6.36	0.42	0.62	0.85
ALI	24	0.69	27.67	8.12	30.89	7.19	3.23	5.41	6.77	4.90	5.15	0.58	0.78	0.94
ELE	18	0.54	33.17	9.32	40.55	7.73	7.38	9.59	10.94	9.21	6.39	0.41	0.64	0.90
PAN	47	0.78	24.04	8.98	30.31	6.72	6.26	6.94	8.35	6.96	4.14	0.54	0.76	0.89
THR	299	0.47	25.72	9.61	28.70	6.60	2.98	7.61	9.22	6.90	5.83	0.43	0.64	0.89
KOR	125	0.40	25.60	9.46	30.07	5.17	4.47	8.36	9.82	8.49	4.76	0.37	0.56	0.87
LYK	207	0.47	33.99	9.19	37.41	8.94	3.43	7.93	9.90	5.47	7.94	0.48	0.66	0.92
MAR	201	0.25	32.70	10.41	37.78	11.15	5.08	9.68	14.10	7.26	10.92	0.44	0.54	0.83
OIN	44	0.18	31.59	9.33	35.32	7.67	3.73	9.65	11.47	8.77	7.48	0.35	0.49	0.88
PIR	128	0.15	35.33	8.38	50.08	9.77	14.75	15.66	18.91	15.54	9.65	0.28	0.40	0.73
Mean	135	0.44	29.58	9.22	35.30	7.82	5.73	8.95	11.00	8.18	6.86	0.43	0.61	0.87
SD	102	0.21	4.18	0.64	6.52	1.72	3.49	2.72	3.39	2.94	2.16	0.09	0.12	0.06
Mean + 2SD	339	0.85	37.93	10.49	48.35	11.26	12.70	14.38	17.78	14.06	11.19	0.61	0.85	0.99

Table 8. Statistics associated with the reconstructed time series of PM_{10} simulations obtained from the output of the 8 synoptically-clustered trained NNs at each station node (NNC) compared with measured values.

	N	R	μ_O	s_O	μ_P	s_P	b	MAE	RMSE	$RMSE_s$	$RMSE_u$	d_1	d_2	R^2
AGP	304	0.58	32.45	19.18	33.54	11.83	1.09	10.50	15.60	10.17	9.83	0.53	0.71	0.83
ALI	26	0.65	29.42	9.96	31.43	8.67	2.01	6.53	7.96	5.21	6.68	0.58	0.78	0.93
ELE	27	0.73	42.41	15.72	43.62	11.67	1.21	9.13	10.65	7.18	7.86	0.59	0.83	0.94
PAN	49	0.54	25.49	11.46	29.88	9.12	4.39	7.33	10.93	6.65	7.71	0.54	0.70	0.85
THR	329	0.50	30.06	19.93	29.67	9.68	–0.39	9.77	17.27	11.68	9.06	0.50	0.59	0.77
KOR	134	0.42	30.22	26.03	30.05	8.63	–0.17	11.21	23.66	18.06	8.91	0.41	0.43	0.65
LYK	346	0.69	49.23	24.17	43.22	15.46	–6.02	12.10	18.43	13.78	11.20	0.62	0.77	0.89
MAR	304	0.68	46.99	26.28	44.38	18.43	–2.61	12.58	19.49	12.35	13.78	0.63	0.79	0.87
OIN	60	0.54	41.48	23.28	38.87	13.78	–2.61	12.97	19.57	13.18	11.81	0.52	0.67	0.83
PIR	197	0.67	45.86	18.50	51.34	16.00	5.48	11.62	15.17	9.85	11.84	0.56	0.79	0.91
Mean	178	0.60	37.36	19.45	37.60	12.33	0.24	10.37	15.87	10.81	9.87	0.55	0.71	0.85
SD	134	0.10	8.70	5.73	7.73	3.46	3.42	2.18	4.84	3.85	2.24	0.06	0.12	0.09
Mean + 2SD	446	0.80	54.76	30.92	53.07	19.24	7.08	14.74	25.55	18.51	14.35	0.68	0.94	1.00

the case of an NN trained on the 90% of the dataset and also for time series of PM_{10} reconstructed from 8 NNs trained on synoptically-clustered data - with some small improvement with regards to the overall RMSE with the latter. Fig. 5 shows the size of linear and nonlinear average error statistics across the station nodes obtained from NNs trained with and without synoptic clustering.

The largest average error corresponds to the NN trained without synoptic clustering whereby at the KOR station node the RMSE = 25.68 $\mu g\ m^{-3}$ (associated with 134 pairs of

Table 9. Statistics associated with the reconstructed time series of PM_{10} simulations obtained from the output of the 8 synoptically-clustered trained NNs at each station node (NNC) compared with measurements which are below the EU Air Quality Directive limit value of 50 μgm^{-3}.

	N (PM_{10} < 50)	R	μ_O	s_O	μ_P	s_P	b	MAE	RMSE	$RMSE_s$	$RMSE_u$	d_1	d_2	R^2
AGP	258	0.53	25.98	9.40	31.15	9.33	5.17	8.22	10.43	7.94	7.97	0.49	0.68	0.86
ALI	24	0.68	27.67	8.12	30.79	8.36	3.13	6.12	7.14	5.41	6.25	0.57	0.78	0.94
ELE	18	0.53	33.17	9.32	38.68	10.38	5.51	9.08	10.86	4.00	9.03	0.46	0.67	0.90
PAN	47	0.56	24.04	8.98	29.59	9.13	5.55	6.67	10.08	5.55	7.60	0.56	0.70	0.85
THR	299	0.53	25.72	9.61	28.63	8.87	2.91	7.41	9.41	4.95	7.69	0.50	0.71	0.88
KOR	125	0.45	25.60	9.46	29.32	7.80	3.72	7.97	9.83	7.00	6.96	0.45	0.65	0.87
LYK	207	0.52	33.99	9.19	35.68	9.62	1.69	7.37	9.35	4.45	8.23	0.52	0.71	0.93
MAR	201	0.38	32.70	10.41	36.49	12.02	3.80	9.21	13.10	4.41	12.33	0.48	0.62	0.85
OIN	44	0.43	31.59	9.33	35.42	12.78	3.83	9.87	12.63	4.25	11.69	0.47	0.61	0.85
PIR	128	0.39	35.33	8.38	45.20	11.15	9.87	11.81	14.75	9.58	10.26	0.38	0.54	0.83
Mean	135	0.50	29.58	9.22	34.10	9.94	4.52	8.37	10.76	5.75	8.80	0.49	0.67	0.88
SD	102	0.09	4.18	0.64	5.24	1.61	2.24	1.68	2.19	1.85	2.02	0.06	0.07	0.04
Mean + 2SD	339	0.68	37.93	10.49	44.57	13.17	9.00	11.73	15.14	9.45	12.83	0.60	0.80	0.95

Table 10. Statistics associated with simulation across the 10 station nodes with the NN trained without synoptic clustering ("NNU") together with statistics associated with reconstructing and aggregating outputs across the 10 station nodes using the 8 synoptically-clustered NNs ("NNC").

	N	R	μ_O	s_O	μ_P	s_P	b	MAE	RMSE	$RMSE_s$	$RMSE_u$	d_1	d_2	R^2
NNU	1776	0.58	39.31	23.54	38.78	14.30	–0.53	12.21	19.25	13.88	11.87	0.56	0.70	0.82
NNC	1776	0.66	39.31	23.54	38.48	15.71	–0.83	11.13	17.74	9.46	12.41	0.61	0.77	0.85

Table 11. Comparison of the coefficient of determination (R^2) for the multiple lnear regression (MLR) model of PM_{10} using the photochemical input triplet (NO,NO_2,O_3) and the neural network models without synoptic clustering (NNU) and with synoptic clustering (NNC) for each of the 10 stations providing coincident measurement data. For the MLR model the average value of R^2 across the network of stations is reported as the median of the values while for the NNU and NNC, the mean value is reported.

R^2 values	AGP	ALI	ELE	PAN	THR	KOR	LYK	MAR	OIN	PIR	Average
MLR	0.22	0.30	0.25	0.24	0.16	0.07	0.41	0.35	0.05	0.26	0.25
NNU	0.81	0.94	0.92	0.89	0.74	0.58	0.87	0.84	0.79	0.87	0.83
NNC	0.83	0.93	0.94	0.85	0.77	0.65	0.89	0.87	0.83	0.91	0.85

NN estimates and measured daily values). For the 125 data points of this sample where PM_{10} < 50 μg m^{-3} (i.e., below the EU Air Quality Directive limit value) the corresponding RMSE falls to 9.82 μg m^{-3}. For the same input data fed to synoptically-clustered NNs, RMSE = 23.66 μg m^{-3} for the 134 NN estimates and RMSE = 9.83 μg m^{-3} for the 125 data points of this sample where PM_{10} < 50 μg m^{-3}. A similar trend is observed at all station nodes and suggests that the NN model is capturing the bulk of routine values very well (to within ≈ 11 μg m^{-3}). Outlier values (i.e., measurements which are in excess of the limit value) are less well modeled by the NNs. This effect translates into a modulation of the goodness of fit at station nodes such as KOR and OIN where measurements are strongly in excess of the limit value of 50 μg m^{-3} as shown in the lower panels of Fig. 5. To place this effect in context, at the KOR station node, while only 9 out of 134 data points (i.e., 6.7%) are in excess of the EU Air Quality Directive limit value, they have a strong impact on the goodness of fit measures when comparing the whole simulation sample ("All") with the statistics for routine values where PM_{10} < 50 μg m^{-3}. At the LYK station node, where some 40.2% of the simulation data exceed the limit value, the performance of the NNs trained both with and without synoptic clustering is robust for the subset of routine values (below the limit value) as shown in Fig. 6. This gives additional credence to the notion that the NNs perform reliably well for routine values.

To sum up our findings in this section, NN models with synoptic clustering achieved an average root mean square error (RMSE) ≈ 16 μg m^{-3} across the station nodes with an average index of agreement (IA) of 0.71 (somewhat better than the control network whose performance statistics were RMSE ≈ 17 μg m^{-3} and IA = 0.61 respectively). For routine measurements below the EU Air Quality Directive limit value of 50 μg m^{-3}, the average error is as low as RMSE ≈ 11 μg m^{-3} across the station nodes.

CONCLUSIONS

The NN modeling approach developed and tested here for estimating daily PM_{10} concentrations from photochemical measurements can be readily applied to model other PM

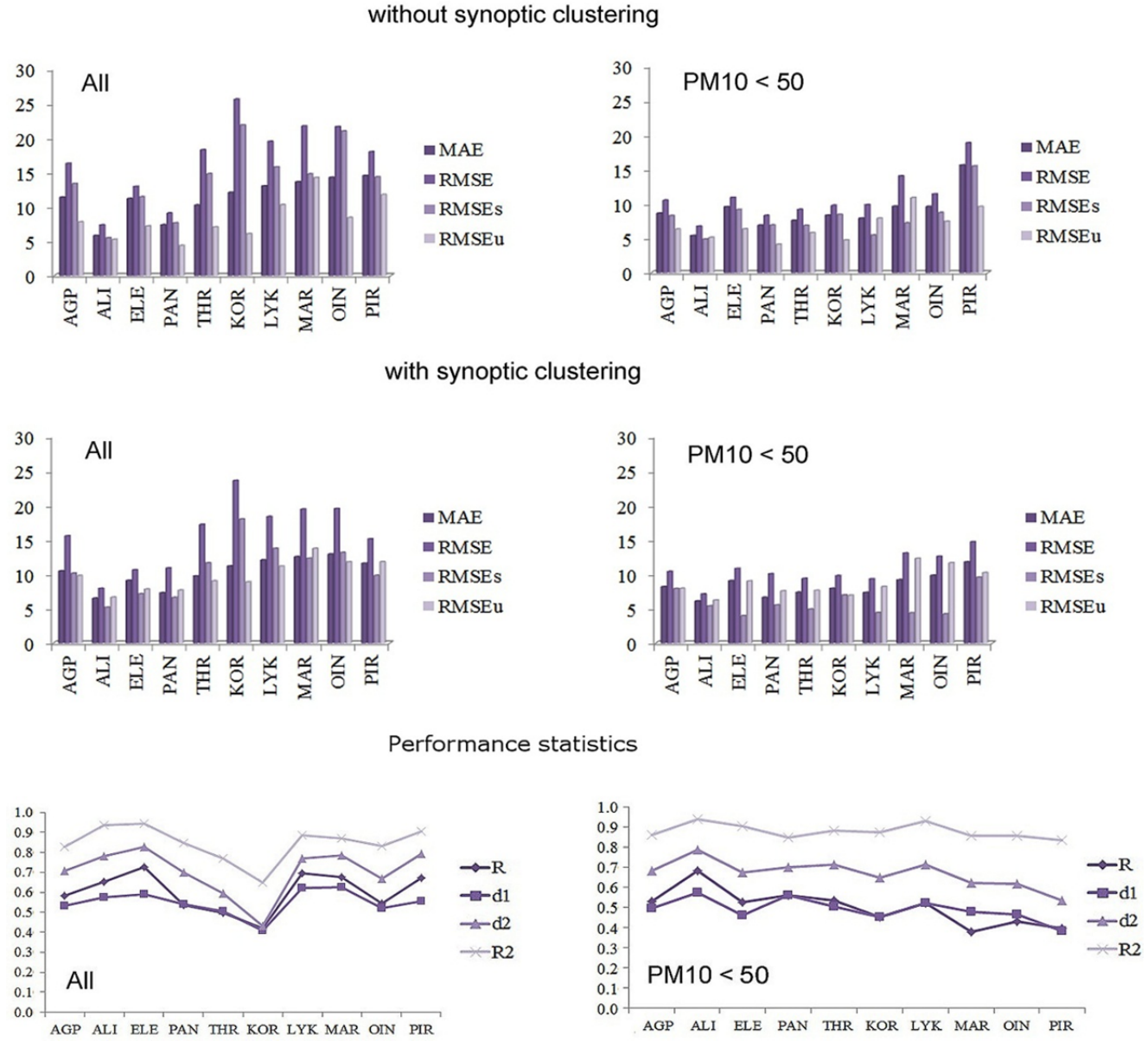

Fig. 5. *Upper Panels:* Linear and nonlinear average error statistics associated with PM_{10} estimates compared with measured values for the NN trained without synoptic clustering values. The average error statistics for measured values of $PM_{10} < 50$ μg m^{-3} is shown at right. *Middle Panels:* Error statistics for the output produced by training a separate NN for each data partition corresponding to a different synoptic cluster. The average error statistics for measured values of $PM_{10} < 50$ μg m^{-3} is shown at right. *Lower Panels*: Linear and nonlinear goodness of fit statistics for the output produced from the 8 synoptic cluster NNs. The goodness of fit statistics for measured values of $PM_{10} < 50$ μg m^{-3} is shown at right.

concentrations such as $PM_{2.5}$ and/or PM_1, and can help increase the spatiotemporal coverage and representivity of existing air quality monitoring networks enabling them to contribute more data to urban, suburban or interurban assessments of PM. The estimated daily values of PM_{10} have average errors small enough (≈ 11 μg m^{-3}) to make such models appear to be operationally feasible. Both NN models with and without synoptic clustering, were found to greatly outperform their linear MLR model counterparts across all sites of the air quality monitoring network. MLR was found to be extremely helpful in helping determine the most relevant chemical species to be included in the model design and, despite the complexity of the NN architecture needed to achieve deep learning (two layers of 30 hidden neurons), Bayesian regularization was found to be instrumental in helping stabilize network learning, avoid overfitting and to maximize the generalization potential of the trained NN models.

A major advantage of the methodology described in this paper is that photochemical data (NO, NO_2 and O_3), unlike PM measurement, is already a feature of most monitoring networks. Furthermore, daily analysis of atmospheric circulation and synoptic pattern categorization is also something readily available and easy to obtain from daily

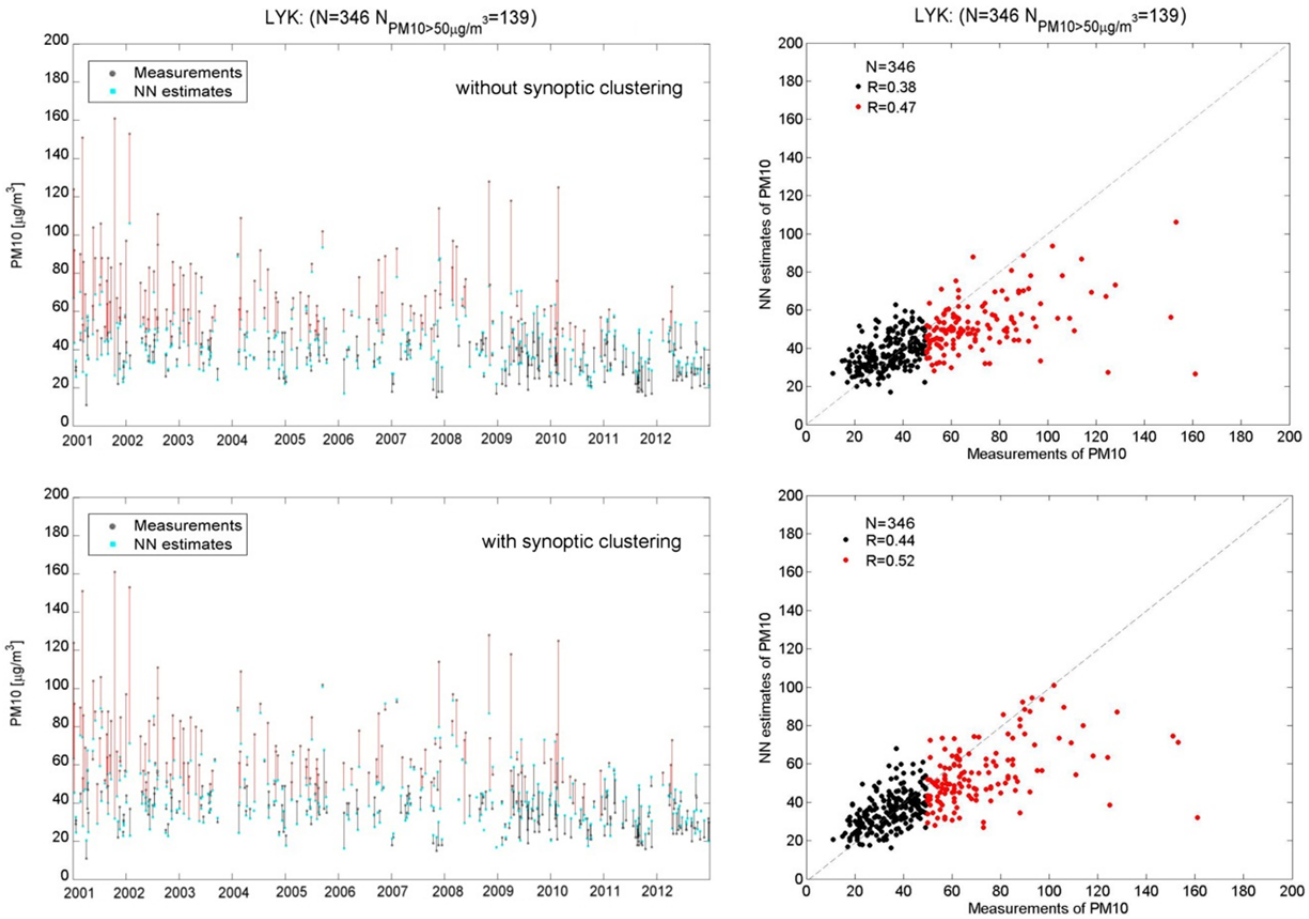

Fig. 6. *Upper:* NN estimates of PM_{10} (cyan) at the LYK station node obtained by the NN trained without synoptic clustering and corresponding measurements (dark grey) connected by black lines when $PM_{10} < 50$ μg m^{-3} and by red lines when $PM_{10} \geq 50$ μg m^{-3}. The right hand panel shows regression of NN estimates on measured values for the case of $PM_{10} \geq 50$ μg m^{-3} (red) and $PM_{10} < 50$ μg m^{-3} (black). *Lower:* As for the upper panels but with NN estimates of PM_{10} obtained by NNs trained with synoptic clustering.

meteorological bulletins. It is envisaged that NN models like the ones developed here can be used: i) to 'fill-in' gaps in PM_{10} time series were only coincident NO, NO_2, and O_3 measurements are available, and ii) to help extend existing time series of PM_{10} (and potentially $PM_{2.5}$ and PM_1 from construction of analogous models) for the development of PM nowcast (1-day ahead forecast) models, and the production of (interpolated) air quality maps of study regions. This spatiotemporal approach therefore has the potential to increase the effectiveness and reach of existing air quality monitoring networks that can support the legislation of environmental policy for engendering behavioural change to reduce air pollution levels.

ACKNOWLEDGMENTS

This work was performed as part of the project "*Design and development of a system to monitor the spatiotemporal evolution of gaseous and particulate air pollution using neural networks*" funded by THESPIA (foundation of synergistic and integrated methodologies and tools for monitoring, managing and forecasting environmental parameters and stresses) under the call "Developmental proposals of Research Agencies - KRIPIS" of the operational programme "Competitiveness and Entrepeneurship". MT would like to thank IERSD-NOA for their kind hospitality during this work. The authors are grateful to the anonymous reviewers for their excellent suggestions and attention to detail, and to the editor Professor Emeritus Philip Hopke whose contributions substantially improved the quality of the manuscript.

DISCLAIMER

While the authors have made every effort to ascertain the validity of all references in the text to air quality as well as potential implications on health, the results presented here should be interpreted as being valid to stated levels of accuracy and acted upon with due caution.

SUPPLEMENTARY MATERIAL

Supplementary data associated with this article can be found in the online version at http://www.aaqr.org.

REFERENCES

Barne, C., Alexis, N.E., Bernstein, J.A., Cohn, J.R., Demain, J.G., Horner, E., Levetin, E., Nei, A. and Phipatanakul, W. (2013). Climate change and our environment: The effect on respiratory and allergic disease. *J. Allergy Clin. Immunol. Pract.* 1: 137–141.

Beale, M.H., Hagan, M.T. and Demuth, H. (2015). Neural Network Toolbox: User's Guide, The MathWorks, 824 Inc., Natick, MA (USA).

Bishop, C.M. (1995). *Neural Networks for Pattern Recognition*. Oxford University Press, New York, USA.

Boezen, H.M., van der Zee, S.C., Postma, D.S., Vonk, J.M., Gerritsen, J., Hoek, G., Brunekreef, B., Rijcken, B. and Schouten, J.P. (1999). Effects of ambient air pollution on upper and lower respiratory symptoms and peak expiratory flow in children. *Lancet* 353: 874–878.

Boyouk, N., Léon, J.F., Delbarre, H., Podvin, T. and Deroo, C. (2010). Impact of the mixing boundary layer on the relationship between $PM_{2.5}$ and aerosol optical thickness. *Atmos. Environ.* 44: 271–277.

Brauer, M., Amann, M., Burnett, R.T., Cohen, A., Dentener, F., Ezzati, M., Henderson, S.B., Krzyzanowski, M., Martin, R.V., Van Dingenen, R., van Donkelaar, A. and Thurston, G.D. (2012). Exposure assessment for estimation of the global burden of disease attributable to outdoor air pollution. *Environ. Sci. Technol.* 46: 652–660.

Chaloulakou, A., Kassomenos, P., Spyrellis, N., Demokritou, P. and Koutrakis, P. (2003a). Measurements of PM_{10} and $PM_{2.5}$ particle concentrations in Athens, Greece. *Atmos. Environ.* 37: 649–660.

Chaloulakou, A., Grivas, G. and Spyrellis, N. (2003b). Neural network and multiple regression models for PM_{10} prediction in Athens: a comparative assessment. *J. Air Waste Manage. Assoc.* 53: 1183–1190.

Cybenko, G. (1989). Approximation by super-positions of a sigmoidal function. *Math. Control Signals Syst.* 2: 303–314.

Davidson, C.I., Phalen, R.F. and Solomon, P.A. (2005). Airborne particulate matter and human health: A review. *Aerosol Sci. Technol.* 39: 737–749.

Dimitriou, K. and Kassomenos, P. (2014). Local and regional sources of fine and coarse particulate matter based on traffic and background monitoring. *Theor. Appl. Climatol.* 116: 413–433.

Dockery, D.W. and Pope, C.A. (1994). Acute respiratory effects of particulate air pollution. *Annu Rev Public Health* 15: 107–132.

Eeftens, M., Tsai, M.Y., Ampe, C., Anwander, B., Beelen, R., Bellander, T., Cesaroni, G., Cirach, M., Cyrys, J., de Hoogh, K., De Nazelle, A., de Vocht, F., Declercq, C., Dėdelė, A., Eriksen, K., Galassi, C., Gražulevičienė, R., Grivas, G., Heinrich, J., Hoffmann, B., Iakovides, M., Ineichen, A., Katsouyanni, K., Korek, M., Krämer, U., Kuhlbusch, T., Lanki, T., Madsen, C., Meliefste, K., Mölter, A., Mosler, G., Nieuwenhuijsen, M., Oldenwening, M., Pennanen, A., Probst-Hensch, N., Quass, U., Raaschou-Nielsen, O., Ranzi, A., Stephanou, E., Sugiri, D., Udvardy, O., Vaskövi, É., Weinmayr, G., Brunekreef, B. and Hoek, G. (2012). Spatial variation of $PM_{2.5}$, PM_{10}, $PM_{2.5}$ absorbance and PM coarse concentrations between and within 20 European study areas and the relationship with NO_2: Results of the ESCAPE project. *Atmos. Environ.* 62: 303–317.

Engel-Cox, J.A., Holloman, C.H., Coutant, B.W. and Hoff, R.M. (2004). Qualitative and quantitative evaluation of MODIS satellite sensor data for regional and urban scale air quality. *Atmos. Environ.* 38: 2495–2509.

Fameli, K., Assimakopoulos, V., Kotroni, V. and Retalis, A. (2013). Effect of the land use change characteristics on the air pollution patterns above the Greater Athens area (GAA) after 2004. *Global NEST J.* 15: 169–177.

Fameli, K.M. and Assimakopoulos, V.D. (2015). Development of a road transport emission inventory for Greece and the Greater Athens Area: effects of important parameters. *Sci. Total Environ.* 505: 770–786.

Gerasopoulos, E., Koulouri, E., Kalivitis, N., Kouvarakis, G., Saarikoski, S., Mäkelä, T., Hillamo, R. and Mihalopoulos, N. (2007). Size-segregated mass distributions of aerosols over Eastern Mediterranean: seasonal variability and comparison with AERONET columnar size-distributions. *Atmos. Chem. Phys*. 7: 2551–2561.

Grantz, D.A., Garner, J.H.B. and Johnson, D.W. (2003). Ecological effects of particulate matter. *Environ. Int.* 29: 213–239.

Grivas, G., Chaloulakou, A. and Kassomenos, P. (2008). An overview of the PM_{10} pollution problem, in the Metropolitan Area of Athens, Greece. Assessment of controlling factors and potential impact of long range transport. *Sci. Total Environ.* 389: 165–177.

Hedegaard, G.B., Christensen, J.H. and Brandt, J. (2013). The relative importance of impacts from climate change vs. emissions change on air pollution levels in the 21st century. *Atmos. Chem. Phys*. 13: 3569–3585.

Hoek, G., Forsberg, B., Borowska, M., Hlawiczka, S., Vaskövi, E., Welinder, H., Branis, M., Benes, I., Kotesovec, F., Otto Hagen, L., Cyrys, J., Jantunen, M., Roemer, W. and Brunekreef, B. (1997). Wintertime PM_{10} and black smoke concentrations across Europe: results from the PEACE study. *Atmos. Environ.* 31: 3609–3622.

Hoff, R.M. and Christopher, S.A. (2009). Remote sensing of particulate pollution from space: have we reached the promised land? *J. Air Waste Manage. Assoc.* 59: 645–675.

Hornik, K., Stinchcombe, M. and White, H. (1989). Multilayer feedforward networks are universal approximators. *Neural Networks* 2: 359–366.

Intergovernmental Panel on Climate Change (IPCC). Climate Change 2013 The Physical Science Basis: Contribution of the Working Group I to the Fifth Assessment Report of the IPCC. Cambridge University Press, New York, 2013.

Kanakidou, M., Mihalopoulos, N., Kindap, T., Im, U., Vrekoussis, M., Gerasopoulos, E., Dermitzaki, E., Unal, A., Koçak, M., Markakis, K., Melas, D., Kouvarakis, G., Youssef, A.F., Richter, A., Hatzianastassiou, N., Hilboll,

A., Ebojie, F., Wittrock, F., von Savigny, C., Burrows, J.P., Ladstaetter-Weissenmayer, A. and Moubasher, H. (2011). Megacities as hot spots of air pollution in the East Mediterranean. *Atmos. Environ.* 45: 1223–1235.

Kassomenos, P., Flocas, H.A., Skouloudis, A.N., Lykoudis, S., Asimakopoulos, V.D. and Petrakis, M., (1998a). Relationship of air quality indicators and synoptic scale circulation at 850 hPa over Athens during 1983-1995. *Environ. Technol.* 19: 13–24.

Kassomenos, P., Flocas, H.A., Lykoudis, S. and Petrakis, M. (1998b). Analysis of mesoscale patterns in relation to synoptic conditions over an urban Mediterranean basin. *Theor. Appl. Climatol.* 59: 215–229.

Kassomenos, P., Gryparis, A., Samoli, E., Katsouyianni, K., Lycoudis, S. and Flocas, H.A. (2001). Atmospheric circulation types and daily mortality in Athens, Greece. *Environ. Health Perspect.*109: 591–596.

Kassomenos, P., Papaloukas, C., Petrakis, M. and Karakitsios, S. (2008). Assessment and prediction of short term hospital admissions: The case of Athens, Greece. *Atmos. Environ.* 42: 7078–7086.

Kassomenos, P.A., Vardoulakis, S., Chaloulakou, A., Paschalidou, A.K., Grivas, G., Borge, R. and Lumbreras, J. (2014). Study of PM_{10} and $PM_{2.5}$ levels in three European cities: Analysis of intra and inter urban variations. *Atmos. Environ.* 87: 153–163.

Kolehmainen, M., Martikainen, H. and Ruuskanen, J. (2001). Neural networks and periodic components used in air quality forecasting. *Atmos. Environ.* 35: 815–825.

Kukkonen, J., Partanen, L., Karppinen, A., Ruuskanen, J., Junninen, H., Kolehmainen, M., Niska, H., Dorling, S., Chatterton, T., Foxall, R. and Cawley, G. (2003). Extensive evaluation of neural network models for the prediction of NO_2 and PM_{10} concentrations, compared with a deterministic modelling system and measurements in central Helsinki. *Atmos. Environ.* 37: 4539–4550.

Kukkonen, J., Pohjola, M., Ssokhi, R., Luhana, L., Kitwiroon, N., Fragkou, L., Rantamaki, M., Berge, E., Odegaard, V. and Havardslordal, L. (2005). Analysis and evaluation of selected local-scale PM_{10} air pollution episodes in four European cities: Helsinki, London, Milan and Oslo. *Atmos. Environ.* 39: 2759–2773.

Liu, Y., Park, R.J., Jacob, D.J., Li, Q., Kilaru, V. and Sarnat, J.A. (2004). Mapping annual mean ground-level $PM_{2.5}$ concentrations using Multiangle Imaging Spectroradiometer aerosol optical thickness over the contiguous United States. *J. Geophys. Res.* 109: D22206.

MacKay, D.J.C. (1992) Bayesian interpolation. *Neural Comp.* 4: 415–447.

Matsumoto, M. and Nishimura, T. (1998): Mersenne twister: A 623-dimensionally equidistributed uniform pseudo-random number generator. *ACM Trans. Model. Comput. Simul.* 8: 3–30.

Michaelides, S., Tymvios, F., Paronis, D. and Retalis, A. (2011). Artificial Neural Networks for the Diagnosis and Prediction of Desert Dust Transport Episodes. In *Soft Computing in Green and Renewable Energy Systems* Springer Berlin, Heidelberg, pp. 285–304.

Michalakakou, G., Flocas, H.A., Santamouris, M. and Helmis, C.G., (2002). The impact of synoptic scale atmospheric circulation on the urban heat island over Athens, Greece. *J. Appl. Met.*, 41: 519–527.

Mues, A., Manders, A., Schaap, M., van Ulft, L.H., van Meijgaard, E. and Builtjes, P. (2013). Differences in particulate matter concentrations between urban and rural regions under current and changing climate conditions. *Atmos. Environ.* 80: 232–247.

Pateraki, S., Asimakopoulos, D.N., Flocas, H.A., Maggos, T. and Vasilakos, C. (2012). The role of meteorology on different sized aerosol fractions (PM_{10}, $PM_{2.5}$, $PM_{2.5–10}$), *Sci. Total Environ.* 419: 124–135.

Pateraki, S., Assimakopoulos, V.D., Maggos, T., Fameli, K.M., Kotroni, V. and Vasilakos, C. (2014). Particulate matter pollution over a Mediterranean urban area. *Sci. Total Environ.* 463–464: 508–524.

Pope III, C.A., Ezzati, M. and Dockery, D.W. (2009). Fine-particulate air pollution and life expectancy in the United States. *N. Engl. J. Med.* 360: 376–386.

Raaschou-Nielsen, O., Andersen, Z.J., Beelen, R., Samoli, E., Stafoggia, M., Weinmayr, G., Hoffmann, B., Fischer, P., Nieuwenhuijsen, M.J., Brunekreef, B., Xun, W.W., Katsouyanni, K., Dimakopoulou, K., Sommar, J., Forsberg, B., Modig, L., Oudin, A., Oftedal, B., Schwarze, P.E., Nafstad, P., De Faire, U., Pedersen, N.L., Östenson, C.G., Fratiglioni, L., Penell, J., Korek, M., Pershagen, G., Eriksen, K.T., Sørensen, M., Tjønneland, A., Ellermann, T., Eeftens, M., Peeters, P.H., Meliefste, K., Wang, M., Bueno-de-Mesquita, B., Key, T.J., de Hoogh, K., Concin, H., Nagel, G., Vilier, A., Grioni, S., Krogh, V., Tsai, M.-Y., Ricceri, F., Sacerdote, C., Galassi, C., Migliore, E., Ranzi, A., Cesaroni, G., Badaloni, C., Forastiere, F., Tamayo, I., Amiano, P., Dorronsoro, M., Trichopoulou, A., Bamia, C., Vineis, P. and Hoek, G. (2013). Air pollution and lung cancer incidence in 17 European cohorts: prospective analyses from the European Study of Cohorts for Air Pollution Effects (ESCAPE). *Lancet Oncol.* 14: 813–822.

Rückerl, R., Schneider, A., Breitner, S., Cyrys, J. and Peters, A. (2011). Health effects of particulate air pollution: A review of epidemiological evidence. *Inhalation Toxicol.* 23: 555–592.

Rumelhart, D.E., Hinton, G.E. and Williams, R.J. (1986). Learning representations by backpropagating errors. *Nature* 323: 533–536.

Samet, J.M., Dominici, F., Curriero, F.C., Coursac, I. and Zeger, S.L. (2000). Fine particulate air pollution and mortality in 20 US cities, 1987–1994. *N. Engl. J. Med.* 343: 1742–1749.

Sen, P.K. (1968). Estimates of the regression coefficient based on Kendall's tau. *J. Am. Stat. Assoc.* 63: 1379–1389.

Sfetsos, A. and Vlachogiannis, D. (2010). A new approach to discovering the causal relationship between meteorological patterns and PM_{10} exceedances. *Atmos. Res.* 98: 500–511.

Snider, G., Weagle, C.L., Martin, R.V., van Donkelaar, A., Conrad, K., Cunningham, D., Gordon, C., Zwicker, M., Akoshile, C., Artaxo, P., Anh, N.X., Brook, J., Dong, J.,

Garland, R.M., Greenwald, R., Griffith, D., He, K., Holben, B.N., Kahn, R., Koren, I., Lagrosas, N., Lestari, P., Ma, Z., Vanderlei Martins, J., Quel, E.J., Rudich, Y., Salam, A., Tripathi, S.N., Yu, C., Zhang, Q., Zhang, Y., Brauer, M., Cohen, A., Gibson, M.D. and Liu, Y. (2015). SPARTAN: A global network to evaluate and enhance satellite-based estimates of ground-level particulate matter for global health applications. *Atmos. Meas. Tech.* 8: 505–521.

Tai, A.P.K., Mickley, L.J., Jacob, D.J., Leibensperger, E.M., Zhang, L., Fisher, J. A. and Pye, H.O.T. (2012). Meteorological modes of variability for fine particulate matter ($PM_{2.5}$) air quality in the United States: implications for $PM_{2.5}$ sensitivity to climate change. *Atmos. Chem. Phys.* 12: 3131–3145.

Taylor, M., Kazadzis, S., Tsekeri, A., Gkikas, A. and Amiridis, V. (2014). Satellite retrieval of aerosol microphysical and optical parameters using neural networks: A new methodology applied to the Sahara desert dust peak. *Atmos. Meas. Tech.* 7: 3151–3175.

Theil, H. (1950). A rank-invariant method of linear and polynomial regression analysis. *Nederl. Akad. Wetensch. Proc.* 53: 386–392.

Unger, N., Bond, T. C., Wang, J. S., Koch, D. M., Menon, S., Shindell, D. T. and Bauer, S. (2010). Attribution of climate forcing to economic sectors. *Proc. Natl. Acad. Sci. U.S.A.* 107: 3382–3387.

van Donkelaar, A., Martin, R.V. and Park, R.J. (2006). Estimating ground-level $PM_{2.5}$ using aerosol optical depth determined from satellite remote sensing. *J. Geophys. Res.* 111: D21201.

van Donkelaar, A., Martin, R.V., Brauer, M., Kahn, R., Levy, R., Verduzco, C. and Villeneuve, P.J. (2010) Global estimates of ambient fine particulate matter concentrations from satellite-based aerosol optical depth: Development and application. *Environ. Health Perspect.* 118: 847–855.

van Poppel, M., Peters, J. and Bleux, N. (2013). Methodology for setup and data processing of mobile air quality measurements to assess the spatial variability of concentrations in urban environments. *Environ. Pollut.* 183: 224–233.

Vardoulakis, S. and Kassomenos, P. (2008). Sources and factors affecting PM_{10} levels in two European cities: implications for local air quality management. *Atmos. Environ.* 42: 3949–3963.

Vrekoussis, M., Richter, A., Hilboll, A., Burrows, J.P., Gerasopoulos, E., Lelieveld, J., Barrie, L., Zerefos, C. and Mihalopoulos, N. (2013). Economic crisis detected from space: Air quality observations over Athens/Greece. *Geophys. Res. Lett.* 40:458–463.

WHO Regional Office for Europe (2013) Review of Evidence on Health Aspects of Air Pollution - REVIHAAP Project. Technical Report. WHO Regional Office for Europe, Copenhagen. http://www.euro.who.int/__data/assets/pdf_file/0004/193108/ (REVIHAAP-Final-technical-report.pdf.

Williams, P.M. (1995). Bayesian regularization and pruning using a Laplace prior. *Neural Comp.* 7: 117–143.

Willmott, C.J., Ackleson, S.G., Davis, R.E., Feddema, J.J., Klink, K.M., Legates, D.R., O'Donnell, J. and Rowe, C.M. (1985). Statistics for the evaluation and comparison of models. *J. Geophys. Res.* 90: 8995–9005.

Xie, Y., Zhao, B., Zhang, L. and Luo, R. (2015). Spatiotemporal variations of $PM_{2.5}$ and PM_{10} concentrations between 31 Chinese cities and their relationships with SO_2, NO_2, CO and O_3. *Particuology* 20: 141–149.

Yuval, Broday, D.M. and Alpert, P. (2012). Exploring the applicability of future air quality predictions based on synoptic system forecasts. *Environ. Pollut.* 166: 65–74.

Zagouras, A., Argiriou, A., Flocas, H.A., Economou, G. and Fotopoulos, S. (2012). An advanced Method for Classifying Atmospheric Circulation Types based on Prototypes Connectivity Graph. *Atmos. Res.* 118: 180–192.

Zeeshan, M. and Oanh, N.K. (2014). Assessment of the relationship between satellite AOD and ground PM_{10} measurement data considering synoptic meteorological patterns and Lidar data. *Sci. Total Environ.* 473: 609–618.

Received for review, December 21, 2015
Revised, April 18, 2016
Accepted, May 23, 2016